PHYSICAL REVIEW B **79**, 085115 (2009)

Positron annihilation study of the electronic structure of URu_2Si_2: Fermi surface and hidden order parameter

M. Biasini*
Department of Physics and Astronomy, University of California-Riverside, Riverside, California 92521, USA and ENEA, Via Martiri di Montesole, 40129 Bologna, Italy

J. Rusz†
Department of Physics, Uppsala University, Box 530, S-751 21 Uppsala, Sweden and Institute of Physics, Academy of Sciences of the Czech Republic, Na Slovance 2, CZ-182 21 Prague, Czech Republic

A. P. Mills, Jr.
Department of Physics and Astronomy, University of California-Riverside, Riverside, California 92521, USA
(Received 22 September 2008; revised manuscript received 18 December 2008; published 19 February 2009)

The Fermi surface (FS) of URu_2Si_2 in the paramagnetic phase has been reinvestigated via the measurement of the two-dimensional angular correlation of the positron annihilation radiation. Unlike previous measurements our experiment provides evidence that density-functional theory gives a fair qualitative description of the FS, showing a large contribution from the $5f$ electrons, although the Fermi volume of electron and hole pockets determined experimentally is smaller than the theoretical description. Furthermore, we propose a method to investigate the nature of the hidden order responsible for the 17.5 K transition.

DOI: 10.1103/PhysRevB.79.085115 PACS number(s): 71.18.+y, 71.27.+a, 71.60.+z, 78.70.Bj

I. INTRODUCTION

The recently observed coexistence of magnetic ordering, superconductivity, and heavy-fermion behavior in some rare-earth and actinide intermetallic compounds has emerged as a central topic of solid-state physics.[1,2] Although these three phenomena had been considered as antagonist one can find a large class of heavy (or moderately heavy) fermions where the strongly correlated state coexists with the magnetic ordering. A notable example is the archetype dense Kondo lattice system CeB_6; other compounds are $CeAl_3$, $CePd_2Si_2$, $CeRh_2Si_2$, UGe_2, URhGe, $U(Ni,Pd)_2Al_3$, $ZrZn_2$, $CeIn_3$, and URu_2Si_2.[3] Among these systems, several have also displayed the fascinating interaction between superconductivity and (anti)ferromagnetism. URu_2Si_2, the first moderately heavy-fermion system showing this variety of phenomena, has been the center of attention of condensed-matter theorists and experimentalists for almost two decades. Extrapolation to 0 K of the paramagnetic regime Sommerfeld coefficient (γ constant) yields $\gamma=180$ mJ/(K^2 mol).[4] Unlike its equally famous $4f$ electron counterpart $CeRu_2Si_2$, which shows neither magnetic ordering nor superconductivity down to temperatures of a few millikelvin, URu_2Si_2 undergoes a second-order transition at $T_1=17.5$ K (Ref. 4) [where the zero-temperature extrapolation of γ decreases to $\simeq 60$ mJ/(K^2 mol)] and a superconducting transition at $T=1.4$ K at ambient pressure. Initially T_1 was ascribed to an antiferromagnetic (AF) transition. However the minuscule moment detected by neutron experiments, $\mu \simeq 0.03\mu_B$,[5] contrasts with the magnitude of the jump in the specific heat across T_1, which would imply an (hypothetical) ordered magnetic moment of about $0.5\mu_B$, and with the value of moment obtained from inverse susceptibility curves on the paramagnetic phase [$\mu_{\text{para}} \cong 1.2\mu_B$ (Ref. 6)]. This large discrepancy aroused several theories[7–12] suggesting a variety of hidden order parameters (HOPs) mainly responsible for the transition. Furthermore, the application of pressure leads to an increase in the value of magnetic moment detected by neutron-scattering experiments, and unlike other examples of magnetically ordered rare-earth compounds (UGa_3 and $CeIn_3$), it leads to an increase in T_1.[6,13] This has suggested that the application of pressure stabilizes a mixed state where the HOP phase may coexist with the AF ordering.[14] As the volume fraction of the AF phase increases as a function of pressure, superconductivity is suppressed, suggesting a link between HOP and superconductivity.[14]

Finally, other authors have suggested the appearance of newer phases generated by the application of large magnetic fields ($B>32$ T), leading to a major reconstruction of the Fermi surface (FS), in a manner similar to the action of the metamagnetic transition on $CeRu_2Si_2$ and UPt_3.[15,16] The Fermi surface (FS) has been studied extensively below the ordered phase and under application of pressure via the de Haas–van Alphen (dHvA) and Shubnikov–de Haas experiments.[16–20] It is worth mentioning that dHvA experiments hardly detected any change in the extremal orbital sections of the FS as a function of pressure.[19]

Low-statistics two-dimensional (2D) angular correlation of the positron annihilation radiation (2D-ACAR) experiments[21] and angle-resolved photoemission spectroscopy (ARPES) experiments[22] have been performed as well. The measurements have been compared to electronic structure calculations based on density-functional theory (DFT) within the usual local-density approximation (LDA) recipe.[18,23] The agreement between 2D-ACAR and ARPES experiments and theory has been rather unsatisfactory.

The purpose of this work has been twofold: (i) to perform high-statistics 2D-ACAR experiments, positioning the sample with the optimal crystal orientation to investigate the theoretical prediction of the FS in the paramagnetic phase.

 ©2009 The American Physical Society

The measurements have been compared to the electronic structure calculated via density-functional theory. The theory has included the calculation of the positron-electron matrix elements; and (ii) to perform an accurate investigation of possible changes in the electronic structure of URu_2Si_2 across the transition, comparing them to those ascribable to the ordering of the hidden parameter based on the theory by Varma and Zhu.[12] It is worth pointing out that in a 2D-ACAR experiment, where the measurements are performed in the presence of a weak magnetic field ($B<1.5$ T), one avoids the disturbances of the ground state caused by considerable Zeeman effect and possible magnetic breakdown due to the strong B fields which need to be applied when the dHvA experiment is performed on heavy fermions. We also note that in materials endowed by a full three-dimensional (3D) $\boldsymbol{k}$ dispersion (such as URu_2Si_2), unlike the case of the 2D-ACAR technique, which determines unambiguously 2D projections of the 3D positron-electron momentum density, ARPES measurements are of difficult interpretation, in particular if they are not aided by a proper calculation of the radiation-electron matrix elements.

In detail, by measuring the distribution $N(\theta_x,\theta_y)$ of the deviation angles from anticollinearity of the annihilation γ rays, a 2D-ACAR experiment determines a 2D projection $[\rho_{2D}^{ep}(p_x,p_y)]$ of the 3D electron-positron (ep) momentum density, $\rho^{ep}(\boldsymbol{p})$,[24] which can be expressed in the single-particle approximation as

$$\rho^{ep}(\boldsymbol{p}) \propto \sum_{n,\boldsymbol{k}}^{occ} \left| \int d\boldsymbol{r}\, \exp(-i\boldsymbol{p}\cdot\boldsymbol{r})\psi_{\boldsymbol{k}}^{n}(\boldsymbol{r})\phi^{\star}(\boldsymbol{r})\sqrt{g(\boldsymbol{r})} \right|^2. \quad (1)$$

Here $\psi_{\boldsymbol{k}}^{n}$ and ϕ denote the electron and positron wave function, respectively, and the summation extends over all occupied $\boldsymbol{k}$ electron states from bands of index n.[24] The enhancement factor[25] $g(\boldsymbol{r})$, a function of the total electronic density $n(\boldsymbol{r})$ $\{g(\boldsymbol{r})\equiv g[n(\boldsymbol{r})]\}$, describes the enhancement of the electronic density at the positron location due to the Coulomb force.

The contribution to $\rho^{ep}(\boldsymbol{p})$ from the conduction bands l is discontinuous at points $\boldsymbol{p}_{F_l}=(\boldsymbol{k}_{F_l}+\boldsymbol{G})$, where $\boldsymbol{G}$ is a reciprocal-lattice vector and $\boldsymbol{k}_{F_l}$ are the reduced Fermi wave vectors in the first Brillouin zone (BZ). The standard Lock-Crisp-West (LCW) transformation,[26] extensively used in the data analysis of 2D-ACAR spectra, reinforces these discontinuities by folding the momentum distribution $\rho^{ep}(\boldsymbol{p})$ back onto the first BZ by translation over the appropriate vectors $\boldsymbol{G}$. If the summation is performed over a sufficient portion of momentum space, the result is[27]

$$\rho_{LCW}^{ep}(\boldsymbol{k}) = \sum_{n} \theta(E_F-\epsilon_{\boldsymbol{k},n}) \int |\psi_{\boldsymbol{k}}^{n}(\boldsymbol{r})|^2 |\phi(\boldsymbol{r})|^2 g_{\boldsymbol{k}}^{n}(\boldsymbol{r})d\boldsymbol{r}. \quad (2)$$

Here ϕ denotes the positron wave function and $\epsilon_{\boldsymbol{k},n}$ is the energy eigenvalue of the electron from band n with Bloch wave vector $\boldsymbol{k}$ and wave function $\psi_{\boldsymbol{k}}^{n}$. The factor $g_{\boldsymbol{k}}^{n}(\boldsymbol{r})$ accounts for the ep correlations.[28] In general, although the mapping of the FS is facilitated when the overlap integral in Eq. (2) is a weakly varying function of $\boldsymbol{k}$, the FS discontinuities [marked by the step function of Eq. (2)] are not shifted by this $\boldsymbol{k}$ dependence.[29] If, as in the present case, the LCW transformation is applied to a projection of $\rho^{ep}(\boldsymbol{p})$, the result of Eq. (2) yields a projection of the electron-positron $\boldsymbol{k}$-space density in the BZ, and consequently, information on the Fermi volume.

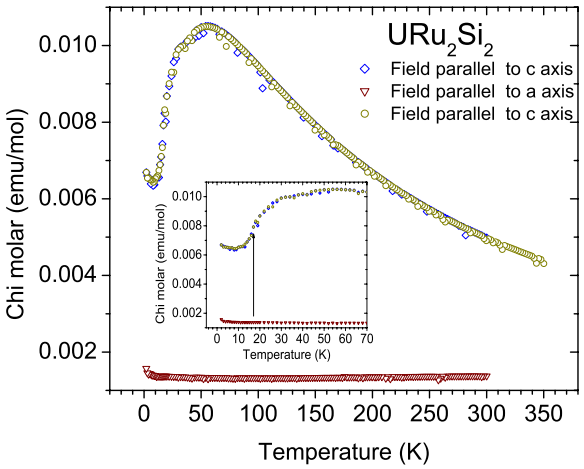

FIG. 1. (Color online) Molar susceptibility of URu_2Si_2 for magnetic field parallel to the a and c axes, respectively. The arrow in the inset shows the change in slope addressed as T_1.

In Refs. 30 and 31 we have presented an algorithm, based on the full-potential linearized augmented plane-wave (FP-LAPW) method implemented in the WIEN2K package,[32] to calculate directly the LCW density via Eq. (2). The method includes electron-positron correlation effects[25] and can treat spin polarized systems.[33,34]

In this work, we present the results of 2D-ACAR measurements over one single crystal of URu_2Si_2 and compare them to our calculations which treat the $5f$ electrons under different starting assumptions. We discuss our results in light of previous dHvA experiments and calculations. Furthermore we discuss the effect of one candidate model of the HOP (Ref. 12) on the outcome of the experiment across T_1 and set the conditions for its observability.

II. EXPERIMENTAL PROCEDURES AND DETAILS OF THE CALCULATIONS

The crystal structures of URu_2Si_2 is body-centered tetragonal (bct), containing one molecule per primitive cell. The space group is $I4/mmm$.

The single crystal was grown by Menovsky from the University of Leiden. It was from the same batch as the one used in Ref. 35. The lattice constants were $a=4.125$ Å and $c=9.575$ Å.

An x-ray diffraction experiment, using the von Laue technique in back reflection, confirmed the final single-crystalline state. The good quality of our single crystal was also confirmed by showing the expected large anisotropy in the magnetization [as measured by a superconducting quantum interference device (SQUID) magnetometer]. The plot of the molar susceptibility for magnetic field parallel to the a and c axes, fully consistent with previous measurements,[4] is shown in Fig. 1.

The measurements were carried out with a recently implemented setup based on a pair of Anger cameras. Each detector comprised a 52 cm diameter and 1.25-cm-thick Na(I) crystal scintillator, optically coupled to a close-packed honeycomb array of 91 photomultipliers. A 10.9 m sample-detector distance provided a coincidence angular view of 52.5×52.5 mrad^2 (1 mrad is equivalent to 0.137 momentum a.u.) in a 272×272 matrix. At this distance the optical angular resolution was 0.6 mrad. The resolving coincidence time for the photon pair selection was 60 ns. A 1.3 T water-cooled electromagnet was employed to focus the positrons, emitted by 0.74 GBq of ^{22}Na, onto the sample. The smearing due to the thermal motion of the positron ($\simeq$0.09 mrad at 9 K and $\simeq$0.16 mrad at 25 K) was negligible compared to the optical resolution. Therefore, the overall experimental resolution, determined by combining the optical resolution with the intrinsic sizes of the positron source spot at the sample, was 0.082 and 0.126 a.u. for the p_x and p_y directions, respectively.

The sample holder consisted of a thick tungsten-based collimator connected directly to the cold finger of the continuous flow He cryostat. The collimator, surrounding entirely the source-sample system, had the double purpose of shielding the detectors from any radiation not emitted directly from the samples and ensuring that the sample temperature was within $\simeq$1 K of the two temperature sensors positioned in the collimator at either sides from the sample position. Several spectra were acquired at T=9 K, T=25 K, and T=45 K. At each temperature $\approx 8 \times 10^8$ raw coincidence counts were collected. The spectra were subjected to the usual correction procedures.[24]

We performed electronic structure calculations regarding the 5f electrons either as ordinary band electrons (f band) or as core states (f core). The f-core calculation was accomplished by forcing a U $5f^3$ core configuration. The energy parameter for the LAPW linearization of the 5f orbitals was set at very a high value ($\sim$2 Ry), thus excluding the U f component from the valence states. The LDA exchange-correlation functional was employed. The self-consistent calculation was performed including spin-orbit coupling at each variational step. The structure parameters mentioned above were employed. The $R_{\mathrm{MT}}K_{\max}$ parameter controlling the basis size was 7.5, which gives above 90 basis functions per atoms.

The evaluation of LCW density was done on equally spaced 726 mesh points in the irreducible wedge of the first BZ. This corresponds to 5133 $\boldsymbol{k}$ points in the full first BZ. The first BZ of URu_2Si_2 (bct structure) in a repeated zone scheme is shown if Fig. 2. The integral in Eq. (2) was evaluated on a regular mesh in the real-space cell of size up to $80 \times 80 \times 180$ (the real number of mesh points was reduced by taking advantage of the crystal symmetry). We have carefully checked that with these calculational parameters all presented results are well converged.

III. RESULTS AND DISCUSSION

A. Paramagnetic phase

The LDA calculation of the band structure and FS in the paramagnetic phase (f-band model) is in reasonable agreement with previous literature[18,23] and in good correspondence with a recent calculation.[36] Figure 3 shows the band structure along high-symmetry directions of the BZ. Furthermore, in Fig. 3 the width of the lines representative of the energy values is set to be proportional to the f orbital character of the $\boldsymbol{k}$ state inside the U sphere. As usual for systems with incompletely occupied f shells, LDA yields a considerable f weight for states near the Fermi level.

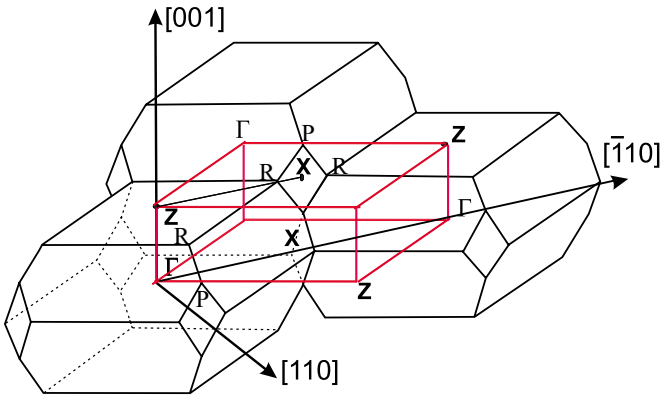

FIG. 2. (Color online) Brillouin zone of URu_2Si_2 in a repeated zone scheme. Letters label the high-symmetry points. The prism (online red color) refers to the nonprimitive part of the BZ of Fig. 4.

The FS, shown in Fig. 4 in a nonprimitive cell of size $\frac{2\pi^2}{a} \times \frac{2\pi}{c}$, consists of two electron pockets (labels a and b, centered at the Γ point with an additional pocket centered at X) and two holelike pockets (c and d) centered at the Z point of the BZ (see Fig. 2 for the position of the cell in the BZ). The electron and hole pockets, listed by letters a, b, c, and d, respectively, are generated by the conduction bands labeled by the same letters in Fig. 3.

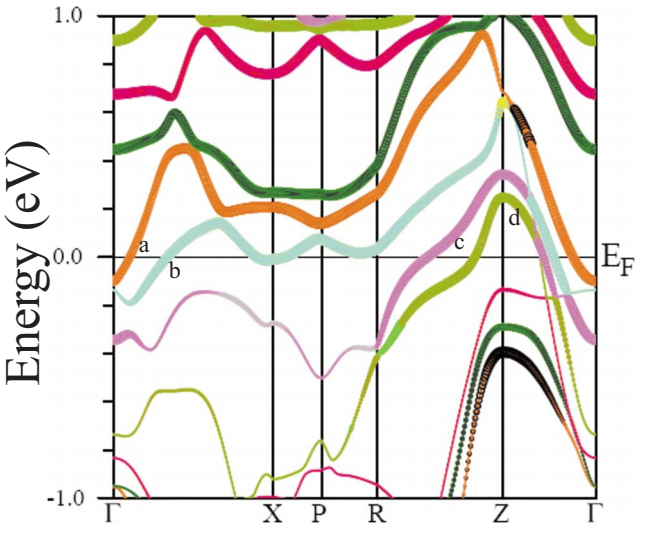

FIG. 3. (Color online) The energy bands of URu_2Si_2 calculated with a self-consistent FP-LAPW calculation along high-symmetry directions of the BZ. All the energies are referred to the Fermi level, set to zero. The width of the lines is set to be proportional to the f orbital character inside the U sphere. The letters a, b, c, and d link the conduction bands to the corresponding FS manifolds labeled as a, b, c, and d in Fig. 4.

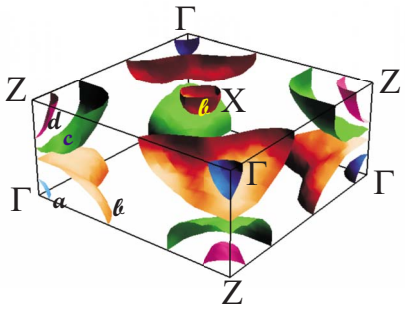

FIG. 4. (Color online) The four Fermi-surface sheets of URu_2Si_2 a, b, c, and d in a nonprimitive cell of size $\frac{2\pi^2}{a} \times \frac{2\pi}{c}$. Capital letters denote high-symmetry points. See Fig. 2 to locate the position of the prism in the BZ of the bct BZ.

Like its $4f$ electron heavy-fermion counterpart $CeRu_2Si_2$, URu_2Si_2 is a compensated metal with equal volumes enclosed by electronlike and holelike FSs. Table I shows the Fermi volume fractions relating to each FS manifold. The Fermi volumes fulfill the compensation requirements within $\simeq 2\%$. In the right column of Table I we also show the calculated dHvA frequencies of the extremal cross-sectional areas of the four FS sheets perpendicular to the [001] direction for a hypothetical experiment performed in the paramagnetic phase. The values are consistent with the calculation reported in Ref. 18 but not with the dHvA experiments which have been performed below T_1.

The topology of the FS dictated a projection direction along the [110]-like axis, which preserves most of the signal coming from electronlike and holelike pockets, avoiding the deleterious superposition and consequent signal cancellation of the FS sheets for integration along [100] or [001]. The estimated overall asymmetric experimental resolution corresponded to 22% and 11% of the corresponding linear sizes of the projected BZ (parallel to the [110] and [001] directions, respectively).

In the 2D-ACAR studies it is common practice to perform a preliminary analysis of the anisotropy $A(p_x,p_y)$ of the angular-correlation spectra. This is defined as

$$A(p_x,p_y) = \rho_{2D}^{ep}(p_x,p_y) - \langle \rho_{2D}^{ep}(p_r) \rangle, \tag{3}$$

where $\rho_{2D}^{ep}(p_x,p_y)$ is the experimental spectrum and

TABLE I. Fermi volumes expressed in % of the BZ [Fermi volume (FV) (BZ %)] of the four conduction bands obtained from the paramagnetic f-band calculation. The increasing number of the bands refers to the increasing energy of the eigenstates. Letters a,b,c,d refer to the labeling shown in Figs. 3 and 4. The right column shows the dHvA frequencies (in G) pertaining to the extremal cross-sectional areas of the FS manifolds perpendicular to the [001] direction.

Band no.	Electron/hole	Sheet	FV (BZ %)	dHvA [001] direction (G)
29	Electron	a	0.4	5.58×10^6
28	Electron	b	11.0	8.76×10^7, 4.52×10^6
27	Hole	c	10.5	7.67×10^7
26	Hole	d	1.1	1.39×10^7

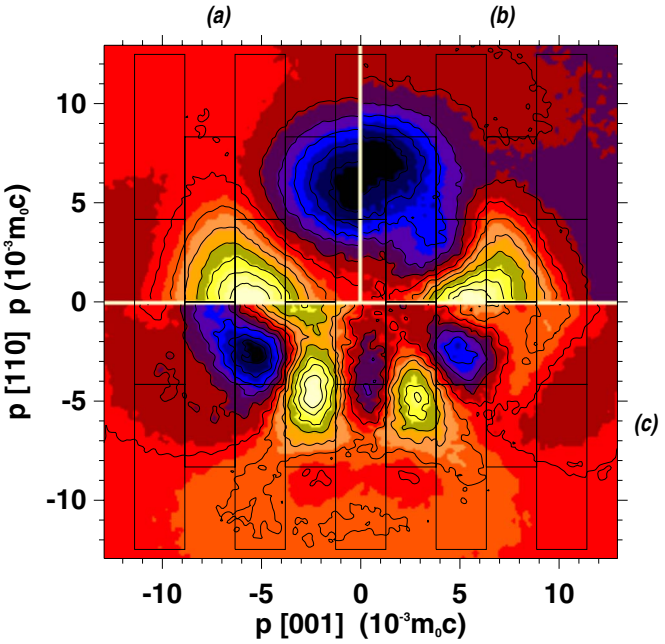

FIG. 5. (Color online) (a) Anisotropy of the measured electron-positron momentum distribution $\rho^{ep}(\boldsymbol{p})$ of $CeRu_2Si_2$ for integration along the $[\bar{1}10]$ direction. The spectrum was smoothed with an equally weighted smoothing array of (0.1×0.1) a.u.^{2}. The borders of the projected first BZ in a repeated zone scheme are shown. (b) Same as (a) for $LaRu_2Si_2$. (c) Same as (a) for URu_2Si_2. In this and all the following grayscale figures white (light color) corresponds to high intensity and black (dark color) to low intensity. 1 momentum a.u.$=7.3 \times 10^{-3} m_0 c$, where m_0 is the electron rest mass and c is the speed of light.

$$\langle \rho_{2D}^{ep}(p_r) \rangle = \frac{1}{2\pi} \int_0^{2\pi} \rho_{2D}^{ep}[p_r \cos(\theta), p_r \sin(\theta)] d\theta$$

represents its angular average. Beyond checking the integrity and proper symmetry of the data, $A(p_x,p_y)$ gives information on the FS topology whenever the anisotropy of the projected electron-positron momentum density, $\rho_{2D}^{ep}(p_x,p_y)$, is mostly caused by the discontinuities of the electron momentum density of the conduction band at the $\boldsymbol{k}_F+\boldsymbol{G}$ points. These discontinuities occur along directions which have the BZ rather than the radial symmetry. In this case it is interesting to compare the radial anisotropy of URu_2Si_2 with that of the isostructural and $4f$ electron heavy-fermion system $CeRu_2Si_2$ and that of the isostructural non-f-electron system $LaRu_2Si_2$, which is measured by one of us (M.B.) with an equivalent 2D-ACAR setup.[37] The lattice constants of the three compounds differ by less than 3%.

Figure 5 shows the anisotropy part of the (110) projection for the aforementioned compounds (data for URu_2Si_2 are not symmetrized). The amplitude variation in the radial anisotropy of URu_2Si_2 corresponds to $\simeq 3\%$ of the maximum, which is equivalent to ~ 21 times the statistical uncertainty of the maximum. The anisotropy of URu_2Si_2, in particular the maxima at (3,5) mrad, is in good agreement with that of the low-intensity spectrum shown in Fig. 2c of Ref. 21. On the other hand, we note that the anisotropy of URu_2Si_2,

mostly concentrated in the low-momentum region and rich with details, contrasts greatly with those of $CeRu_2Si_2$ and $LaRu_2Si_2$, which are rather similar and show coarse structures extending up to large momenta. We also note that unlike the sparse features of $CeRu_2Si_2$ and $LaRu_2Si_2$ the distance between the two symmetric maxima at $\simeq(3,5)$ mrad and their positions is commensurate with the projected reciprocal-lattice vectors, suggesting a link with direct features of the conduction-valence electrons. It is tempting to ascribe the differences among the three spectra as due to the different roles played by the $5f$ electrons in URu_2Si_2, more delocalized and extended in configuration space and consequently more bounded to low values in momentum space, compared to that of the $4f$ electrons of $CeRu_2Si_2$, which are notoriously at the border between localization and itinerancy and are hardly discernible as proven by the similarity between the anisotropy of $CeRu_2Si_2$ and $LaRu_2Si_2$. Furthermore, the large difference between the anisotropies of $CeRu_2Si_2$ and URu_2Si_2 and the close similarity of those of $CeRu_2Si_2$ and $LaRu_2Si_2$(which has no f electrons) reinforce our doubts, proposed in Ref. 37, on the itinerancy of the $4f$ electrons of $CeRu_2Si_2$. Indeed, although the $4f$ electron itinerancy has often been invoked as a typical manifestation of the archetype heavy-fermion behavior,[1,38] several experiments have been inconsistent with this assumption [see, for example, our works on CeB_6 (Ref. 39) and $CeIn_3$ (Ref. 40)].

In summary, the comparison of the radial anisotropy of URu_2Si_2 with those of $CeRu_2Si_2$ and $LaRu_2Si_2$ is in favor of a considerable itinerant character of the $5f$ electrons in URu_2Si_2. If an f orbital character is present in the conduction (or valence) electron wave functions, a $\boldsymbol{k}$ dependence in the overlap integral of Eq. (2), caused by the different degrees of hybridization along the band, may be expected. Indeed a strong positron distortion, which obscured dramatically the FS signals, was observed in two $5f$ electron itinerant systems of simpler [UGa_3 (Ref. 30)] and more complex [UGe_2 (Ref. 33)] crystal structure. It is therefore essential to compare the (projected) experimental LCW density with the corresponding calculated $\rho_{\mathrm{LCW}}^{\mathrm{ep_{calc}}}(\boldsymbol{k})$ which includes the positron-electron matrix elements. Figures 6(a) and 6(c) show the calculated (f band) and experimental projected LCW density, respectively. The total amplitude variation in the unsymmetrized experimental LCW density was $\sim$1.8%, which is equivalent to $\sim$40 times the statistical error of the maximum. Moreover, Fig. 6(b) shows the calculated projected band occupancy, which is uniquely depending on the FS topology. Differences between panels a and b are then ascribed to the effect of the positron wave function and the electron-positron correlations. To make the comparison between theory [Fig. 6(a)] and experiment [Fig. 6(c)] more effective, we perturbed the theory with the same level of noise as the experimental results.

Interestingly, the similarity between the two upper quadrants highlights a very moderate positron wave-function distortion of the FS in this material. This is somehow surprising if compared to the other 2D-ACAR studies of $5f$ electron systems mentioned above. On the whole, there is a fair qualitative agreement between experiment and f-band theory. In fact, the f-band model fares much better than the f-core model, which appears in Fig. 6(d) (only the calculated LCW density is shown). The FS yielded by the f-core model for URu_2Si_2 is rather similar to that predicted for the isostructural non-f-electron system $LaRu_2Si_2$ which, unlike URu_2Si_2, is an uncompensated metal.[37,41] It consists of three small Z-centered holelike pockets surrounded by a much larger holelike manifold (the last FS volume accounting to 45.8% of the BZ volume) and a small roughly cylindrical electronlike FS (cylinder axis along [001]). The overall Fermi volume is equivalent to 53.45% and 3.45% of the BZ volume for the holelike part and electronlike part, respectively[42] (very similar results are obtained for $LaRu_2Si_2$). Even if the hole pockets of the f-core model, similar to the f-band case, generate a minimum at the RZ point projected [see Fig. 6(d)], the shape of that minimum is inconsistent with the experimental results. In general, the overall shape of the contour lines of the f-core model deviates significantly from the experimental result [compare the large fraction of contour lines of the f-core model, almost parallel to the ΓX-ΓX direction, to the large fraction of contour lines of the experiment—Fig. 6(c)], almost perpendicular to that direction. This finding, combined with the striking differences in the radial anisotropy shown in Fig. 5, reinforces the idea of the itinerant character of the $5f$ electrons in URu_2Si_2.

On the other hand, it is worth noting some clear differences between the prediction of LDA (f band) and the experiment. In particular, the maximum at the center of the projected BZ of the experimental data [Fig. 6(c)] is narrower than that of the calculated LCW density [Fig. 6(a)], in particular along the [110] direction. Since the calculated maximum originates from the projection of the Γ-centered electron FS pockets (labeled by letters a and b in Fig. 4), the reduced extent of the experimental maximum suggests a reduction in the Fermi volume compared to the LDA predictions. Note that we cannot compare the experimental LCW density to the projected occupancy [Fig. 6(b)] since the comparison would be strongly affected by positron wave-function effects.

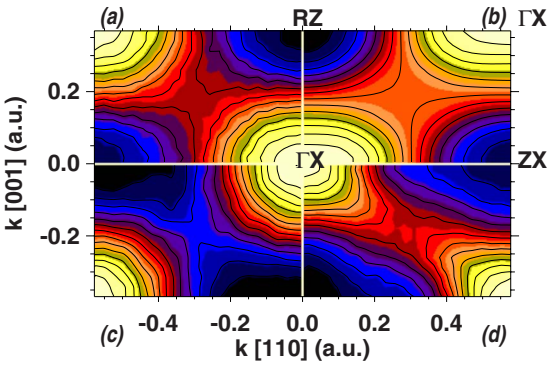

FIG. 6. (Color online) (a) Calculated $\rho_{\mathrm{LCW}}^{\mathrm{ep}}(\boldsymbol{k})$ for the f-band model projected along the [110]-like direction and convoluted with the experimental resolution. A noise level analogous to the statistical precision of the experimental spectra shown in (c) (lower) panel was applied. (b) Same as (a) for the electron occupancy without noise propagation. The theoretical spectra were convoluted with the experimental resolution. (c) Projected experimental LCW density. (d) Same as (a) for the f-core model. The labeling describes the projected BZ high-symmetry points

A rough estimate of the reduction in the Fermi volume can be attained by these steps. (i) The evaluation of the full width at half maximum (FWHM) of the central peak of $\rho^{ep}_{LCW}(\boldsymbol{k})$ in Fig. 6(a), mostly due to the b electron pocket of Fig. 4 and the corresponding evaluation of the peak in Fig. 6(c), yields $FWHM_{calc}=(0.52,0.37)$ a.u. for the [110] and [001] directions and $FWHM_{expt}=(0.43\pm0.04,\ 0.40\pm0.04)$ a.u., respectively. (ii) If one approximates the FS pockets to prolate ellipsoids, integrated along one of the two equivalent directions ([110]-like), the ratio of the corresponding FWHM (experimental over predicted by LDA) is directly proportional to the ratio of the corresponding ellipsoid sizes (this was confirmed by a simple simulation). Therefore one can estimate the ratio of the experimental electron Fermi volume to the one predicted by LDA as $R=\frac{0.45^2\times0.40}{0.52^2\times0.37}\simeq(74\pm10)\%$. (iii) Using the theoretical results from Table I, the experimental Fermi volume turns out to be $FV_{expt}=(0.17\pm0.02)$ electron.

One should note that an adjustment of the theory to yield such Fermi volume reduction cannot simply be attained by shifting the Fermi level upward since this action would not preserve the equality of electron-hole Fermi volume. In fact, the operation of shifting the Fermi level (which is linked to the correct number of electrons per cell) should actually be replaced by shifts of the bands relative to each other, in such a way as to simulate the (unknown) self-energy corrections of the different electron states. In this regard, one should recall that there is no guarantee that LDA eigenvalues reproduce correctly the quasiparticle excitations of the system. Indeed, states with different orbital characters may need different self-energy corrections, leading to modifications of the LDA band structure (see Ref. 43 for the limiting case of oxides). This is certainly the case of *d*-derived bands nearby E_F such as those produced by the Ru (but also U) *d* states.

Consequently, due to the compensation requirements, the same Fermi volume should be inferred for the holelike part of the FS. The dHvA frequency for the extremal cross-sectional area of the reduced electron pocket size is $F_r=(6.0\pm0.7)\times10^7$ G. This value is much larger than any dHvA frequency observed (all dHvA experiments have been performed below T_1). Therefore, the modest reduction in the Fermi volume of the paramagnetic phase suggested by 2D-ACAR is still incompatible with a paramagneticlike Fermi surface below T_1.

B. Low-temperature phase

The last part of this work pertains to the efforts to monitor eventual changes in the electronic structure across T_1. Although most of the experimental evidence is inconsistent with a pure AF state at ambient pressure, we thought that it is appropriate to start this discussion considering the effect of the onset of the AF state on the electronic structure.

We recall that due to the AF order the number of atoms in the unit cell is doubled since the U atoms at position (0,0,0) and $(a/2,a/2,c/2)$ are no longer equivalent. Therefore, in the AF phase, the BZ shrinks to a simple tetragonal cell[44] of sizes $\frac{2\pi}{a}\times\frac{2\pi}{a}\times\frac{2\pi}{c}$. The projected BZ is also reduced to half size as the paramagnetic one. In this case, due to the lower symmetry of the irreducible wedge of the first BZ, the self-consistent calculation was performed on a larger number of mesh points, (2079), corresponding to 28577 $\boldsymbol{k}$ points in the full first BZ.

TABLE II. Experimental dHvA frequencies for B parallel to the [001] direction, from Refs. 17 and 18, the calculated values from Ref. 44, and this work, assuming an antiferromagnetic structure.

Expt. (Ref. 17) (G)	Expt. (Ref. 18) (G)	Theory (Ref. 44) (G)	This work (G)
10.1×10^6	10.5×10^6	10.5×10^6	13.5×10^6
4.1×10^6	4.2×10^6	5.1×10^6	3.65×10^6
	1.9×10^6	4.2×10^6	2.99×10^6

The extension of our scheme to spin polarized calculations is relatively straightforward and described in Refs. 33 and 34. The same steps used in the paramagnetic calculations are done for spin-up and spin-down projections of Bloch states separately.

The AF folding inevitably leads to a considerable decrease in the Fermi volume due to the disappearance of Fermi breaks as a result of the new, more finely spaced, BZ boundaries. As is well known, this happens because some conduction bands (of the paramagnetic phase) develop energy gaps in correspondence of the new BZ boundaries, thus minimizing the total energy. The reduction in the Fermi volume is particularly strong for compensated metals where often holelike FS pockets are folded onto electronlike FS pockets. The Fermi volume calculated from our calculation corresponds to 1.8% of the BZ volume for the electron and hole parts, equivalent to 0.036 electrons and holes per conventional cell, holding 2 f.u. (compare with the paramagnetic values reported in Table I, which refer to the bct cell, holding 1 f.u.). This value is in good agreement with what was reported in Refs. 16 and 45. The dHvA frequencies are considerably reduced as well. They are shown in Table II (column denoted by *this work*) for a B field applied along the [001] direction and compared to the frequencies calculated in Ref. 44 and the experimental values from Refs 17 and 18. The calculated values are in fair agreement with the fully relativistic calculation of Yamagami and Hamada[44] and with the recent calculation of Ref. 36 (the values reported in the table have been estimated visually from Fig. 2 of Ref. 44). There is also a good agreement with the dHvA experiments. Although this positive result is quoted in Ref. 44 we feel that there is an inexplicably insufficient stress in the copious literature to this success of LDA. These results are incompatible with the several experimental works which claim a negligible fraction of the AF phase at ambient pressure. Two possible ways to reconcile the inconsistency are as follows: (i) the FS does not undergo major changes between the AF and the HOP phases and (ii) dHvA detects the FS relating to the AF fraction of the sample (yielding low amplitude of the dHvA oscillations but unchanged frequencies) but does not detect the signal relating to the HOP fraction of the sample. This situation is not uncommon in heavy fermions where the cyclotron mass pertaining to some manifold is very large.[3]

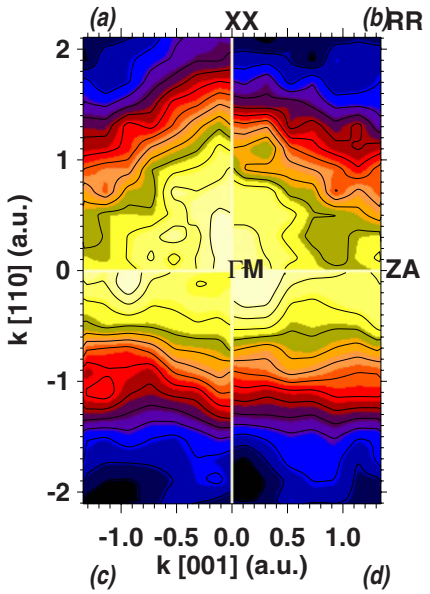

FIG. 7. (Color online) (a) Calculated $\rho^{ep}_{LCW}(\boldsymbol{k})$, for the paramagnetic phase projected along the [110]-like direction and convoluted with the experimental resolution with the additional folding consistent with AF reciprocal-lattice structure. A noise level analogous to that of statistical precision of the experimental spectra shown in the lower panel was applied. (b) Calculated AF $\rho^{ep}_{LCW}(\boldsymbol{k})$. Same noise propagation as in case (a). The theoretical spectra were convoluted with the experimental resolution. (c) Experimental LCW density at $T=25$ K and $T=45$ K summed together and folded according to the AF reciprocal-lattice structure. (d) Same as (c) for data collected at $T=9$ K.

Otherwise, more simply, the HOP is not related to any appreciable static change in the FS and is invisible to dHvA.

To study the effect of the AF ordering on 2D-ACAR experiments it is common practice to fold calculated paramagnetic spectra and experimental ones onto the smaller AF BZ to compare the results with the calculated AF LCW density and experimental low-temperature spectra. Figures 7(a) and 7(b) show calculated paramagnetic and AF spectra, respectively. The theory has been perturbed by statistical noise assuming a large data collection (2×10^9 counts). Clearly, the AF folding makes it extremely difficult to appraise the differences in the electronic structure. The difference between the calculated spectra consists uniquely of a slightly different shape of the broad central maximum, more elongated along the [001] direction and showing a shallow depression at (0,0.1) a.u. for the AF case. The experimental spectra shown in panels (c) and (d) do not confirm this small difference. The contour lines for $k_x<0.1$ a.u. are almost parallel to the [001] direction and inconsistent with the changes shown between panels (a) and (b). It is however rather clear that the precision of our data is insufficient to rule out the AF ordering. Clearly, the discrepancy with the LDA calculation, which was already detected in the paramagnetic phase, is more visible here. However, it is worth recalling that whereas the AF folding causes a large reduction in the amplitude variation in the LCW density (from 1.8% for the paramagnetic case to 0.6% for the antiferromagnetic case), the statistical errors decrease only by a factor of $\sqrt{2}$ (due to the additional folding), and therefore the noise affects the data more strongly.

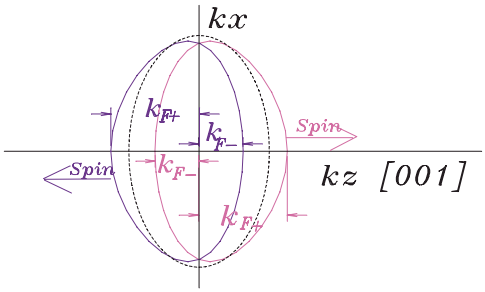

FIG. 8. (Color online) Schematic Fermi surface of URu_2Si_2 for the two different spin directions predicted by Varma and Zhu (Ref. 12) below T_1 (see text). The dotted line denotes the Fermi surface of the paramagnetic phase with vanishing order parameter while the solid lines illustrate the Fermi surface of the helicity-ordered phase (redrawn from Ref. 12).

Several models have been proposed for HOP responsible for the T_1 transition—incommensurate antiferromagnetism,[9] crystalline-electric-field induced multipolar ordering,[8,10] onset of spin-density waves,[46] and FS nesting.[47] The model from Varma and Zhu[12] proposed a transition to an helicity-ordered state, characterized by the splitting of the FS of the paramagnetic phase in two FS manifolds, each having its spin-quantization axis fixed in relation to the Fermi surface (see Fig. 8) with the two FS manifolds becoming asymmetric along the [001] (z) direction. The model predicts that k_{F^+} differs from k_{F^-} by $\cong5\%$, corresponding to a deviation of 0.014 a.u which is within the reach of our spectrometer. We have attempted to foresee the effect of the broken symmetry of the FS proposed in Fig. 8 on a 2D-ACAR experiment which is well suited to test this effect. This happens because positrons emitted in the β^+ decay of various radioactive sources are produced with a partial polarization, p, along the direction of their motion. For a ^{22}Na β^+ source when positrons emitted from one side of the source are collected by the sample, the predicted average polarization of the positrons entering the sample is about $p\cong36\%$.

Experiments of the two γ annihilation rates of positronium in α quartz in the presence of a magnetic field parallel or antiparallel to the direction of the positron polarization (set by the source-sample direction) have confirmed an average polarization of $p\cong31\%$. Polarized positrons will then undergo two γ annihilations in the sample only with electrons of one of the two FS manifolds (up or down) sketched in Fig. 8. Consequently it is possible to detect the predicted asymmetry in the radius of the FS along the c axis.

The response of a 2D-ACAR experiment is strongly dependent to whether the predicted splitting will be realized as single or a multiple domain. In principle, the experiment is able to detect both possibilities, although the latter case requires much larger statistical accuracy to be visible. In the single-domain case, at the onset of the broken-symmetry state, there would be an imbalance in the annihilation rate along the k_z direction (with z along the [001] direction) since $k_{FS_{z^+}}$ is larger than $k_{FS_{z^-}}$. The effect would essentially result in a shift of the centroid of the LCW density on going across

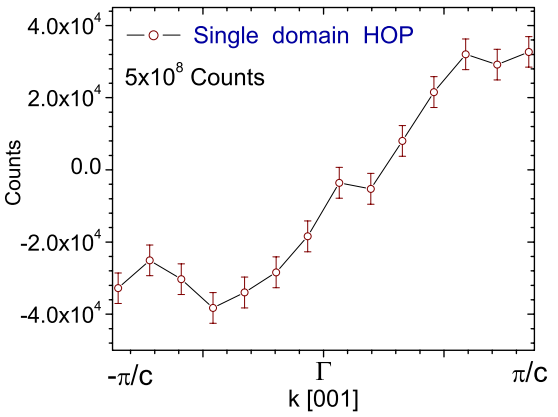

FIG. 9. (Color online) Simulation of the difference between paramagnetic LCW density (DFT calculation) and the low-temperature phase predicted in Ref. 12. The low-temperature LCW density has been obtained by manipulating the paramagnetic LCW density as described in text. The 2D projected LCW density has been further integrated along the [110]-like direction. One domain and 5×10^8 data collection have been assumed. The calculated spectra are subjected to statistical noise.

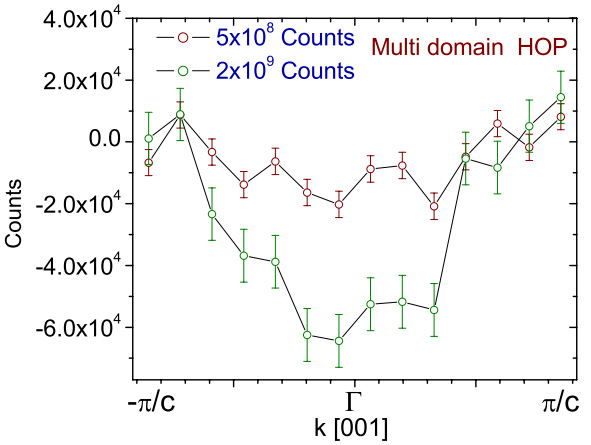

FIG. 10. (Color online) Same as Fig. 9 apart from releasing the assumption that one single domain is formed in the ordered phase (at $T<T_1$). The two calculated LCW densities have been subjected to statistical noise assuming the two levels of data collections listed in the figure.

T_1. In the absence of *ab initio* band-structure calculation of the phase with HOP, we have modeled the effect by shifting the calculated LCW density of AF calculation along the [001] direction by an amount of the order of the asymmetry in the k_{FS_z} radii predicted by Varma and Zhu[12] (we used $\Delta k_{\mathrm{FS}_{z^{\pm}}}\cong 0.02$ a.u.). A realistic positron polarization, $p=30\%$, has been assumed.

Figure 9 shows the difference between paramagnetic state and ordered state prepared as described above for a data collection of 5×10^8 counts. At this statistical level, the difference between the projected LCW densities relating to the two phases is strongly affected by noise. Therefore, we integrated the difference along the [110] direction. The hypothetical asymmetry is clearly above the noise level.

A second possibility of this unknown state of matter is that the new phase does not constitute a single domain. In this case, the suitably polarized positrons should sample both the spin-up and spin-down manifolds symmetrically displaced with respect to the origin. After the realization of the broken-symmetry state the envelope occupied by the two singly-occupied manifolds would be larger and the doubly-integrated LCW density difference with the paramagnetic phase will be depressed at the center. Figure 10 shows the difference between paramagnetic and multidomain ordered states for two levels of data collection. For the changes in k_F consistent with the model[12] Fig. 10 shows that the asymmetry is practically below the threshold of visibility for a realistic data acquisition of 5×10^8 counts and barely visible for a statistic four times larger. At the moment, the investigation across the transition of the twice-integrated LCW density detected a very small difference, which was not entirely reproducible. The smallness of the predicted effect requires an extremely high statistical accuracy and stability which go beyond the previous state of the art. Whereas we cannot exclude that the novel state is realized in multiple domains, since the level of statistical accuracy of the experimental data above and below T_1 is below the 2×10^9 count visibility threshold proposed by the simulation, we can conjecture confidently that in our experiment there is no evidence of the ordered Varma-Zhu state in one single domain.

IV. CONCLUSIONS

We have performed high-statistics 2D-ACAR experiments on a single crystal of URu_2Si_2 in the paramagnetic phase for the [110]-like integration direction. The anisotropy of the data is consistent with previous low statistic data acquisitions[21] and surprisingly different from that of the isostructural $4f$ counterpart $CeRu_2Si_2$ and non-f-electron lanthanide $LaRu_2Si_2$. The anisotropy and the comparison with the LDA-based calculated LCW density suggest that a $5f$ electron itinerant description of the system is adequate.

On the other hand, although LDA provides a fair qualitative agreement with the experiment, we infer a reduction in the Fermi volume predicted by LDA to about $(74\pm10)\%$ of the theoretical one. We have investigated the effect of a pure antiferromagnetic transition below T_1. The experimental data (at ambient pressure) do not support the predictions of the calculated AF LCW density. However the strong reduction in the amplitude variation in the projected LCW density due to the vanishing of a large part of the calculated FS (compared to the paramagnetic phase) would require an extremely high statistical accuracy (obtained by more than 200 days of counting with the current setup) to rule out unambiguously that a large fraction of the sample undergoes AF ordering (at ambient pressure).

Finally, we have simulated the effect of the change in the FS due to helicity-ordered state proposed in Ref. 12, which is suited to be studied with polarized positrons. The comparison between paramagnetic and low-temperature data excludes that this state forms as a single domain. The possibility of a multidomain state, resulting in much weaker difference with respect to the paramagnetic LCW density, would require, as for the AF case, a much larger data collec-

tion and cannot be ruled out on the base of our experiment.

An improvement of the current investigation of the order parameter of URu_2Si_2 will be possible with the predicted upgrade of the apparatus. In fact, a micropositron beam of 25 μm lateral size will make feasible the investigation of hypothetical single domains of the new ordered phase and test much more severely the predicted splitting of the FS.[12] In this case, due to the polarization of the positrons annihilating only with one of the two (up or down) manifolds, it should be possible to observe the asymmetry of the singly-occupied FS along the predicted [001] direction.

ACKNOWLEDGMENTS

We thank Chandra Varma, Peter Oppeneer, Ward Beyermann, David Cassidy, and Sandro Massidda for stimulating discussions and Shi-Hu Deng and Marcus Asaro for help with instrumentation. This work was partly supported by DMEA under Grant No. H9400306206042. The first author would like to thank Berndt Wolf (Physikalisches Institut, Universität Frankfurt, Germany) for providing the URu_2Si_2 crystal used in this experiment, which was grown by A. Menovsky (Amsterdam-Prag).

*Deceased.

†jan.rusz@fysik.uu.se

[1] P. Fulde and G. Zwicknagl, Physica B **206-207**, 125 (1995); G. Zwicknagl, Phys. Scr., T **T49A**, 34 (1993) and references therein.

[2] S. S. Saxena, P. Agarwal, K. Ahilan, F. M. Grosche, R. K. W. Haselwimmer, M. J. Steiner, E. Pugh, I. R. Walker, S. R. Julian, P. Monthoux, G. G. Lonzarich, A. Huxley, I. Sheikin, D. Braithwaite, and J. Flouquet, Nature (London) **406**, 587 (2000) and references therein.

[3] See, for example, Y. Ōnuki and A. Hasegawa, in *Handbook on Physics and Chemistry of Rare Earth* (Elsevier Science, Amsterdam, 1995), Vol. 20, Chap. 135, and references therein.

[4] T. T. Palstra, A. A. Menovsky, J. van den Berg, A. J. Dirkmaat, P. H. Kes, G. J. Nieuwenhuys and J. A. Mydosh, Phys. Rev. Lett. **55**, 2727 (1985).

[5] C. Broholm, J. K. Kjems, W. J. L. Buyers, P. Matthews, T. T. M. Palstra, A. A. Menovsky, and J. A. Mydosh, Phys. Rev. Lett. **58**, 1467 (1987).

[6] H. Amitsuka, M. Sato, N. Metoki, M. Yokoyama, K. Kuwahara, T. Sakakibara, H. Morimoto, S. Kawarazaki, Y. Miyako, and J. A. Mydosh, Phys. Rev. Lett. **83**, 5114 (1999).

[7] H. Ikeda and Y. Ohashi, Phys. Rev. Lett. **81**, 3723 (1998); M. B. Maple, J. W. Chen, Y. Dalichaouch, T. Kohara, C. Rossel, M. S. Torikachvili, M. W. McElfresh, and J. D. Thompson, *ibid.* **56**, 185 (1986).

[8] P. Santini and G. Amoretti, Phys. Rev. Lett. **73**, 1027 (1994).

[9] V. Tripathi, P. Chandra, and P. Coleman, J. Phys.: Condens. Matter **17**, 5285 (2005).

[10] A. Kiss and P. Fazekas, Phys. Rev. B **71**, 054415 (2005).

[11] V. Barzykin and L. P. Gor'kov, Phys. Rev. Lett. **70**, 2479 (1993).

[12] C. M. Varma and Lijun Zhu, Phys. Rev. Lett. **96**, 036405 (2006).

[13] G. Motoyama, T. Nishioka, and N. Sato, Phys. Rev. Lett. **90**, 166402 (2003).

[14] J. R. Jeffries, N. P. Butch, B. T. Yukich, and M. B. Maple, J. Phys.: Condens. Matter **20**, 095225 (2008).

[15] K. H. Kim, N. Harrison, M. Jaime, G. S. Boebinger, and J. A. Mydosh, Phys. Rev. Lett. **91**, 256401 (2003).

[16] Y. J. Jo, L. Balicas, C. Capan, K. Behnia, P. Lejay, J. Flouquet, J. A. Mydosh, and P. Schlottmann, Phys. Rev. Lett. **98**, 166404 (2007).

[17] C. Bergemann, S. R. Julian, G. J. McMullan, B. K. Howard, G. G. Lonzarich, P. Lejay, J. P. Brison, and J. Flouquet, Physica B **230-232**, 348 (1997).

[18] H. Ohkuni, Y. Inada, Y. Tokiwa, K. Sakurai, R. Settai, T. Honma, Y. Haga, E. Yamamoto, Y. Onuki, H. Yamagami, S. Takahashi, and T. Yanagisawa, Philos. Mag. B **79**, 1045 (1999).

[19] M. Nakashima, S. Ikeda, T. Okubo, Y. Inada, R. Settai, H. Ohkuni, E. Yamamoto, Y. Haga, and Y. Onuki, Physica B **329-333**, 566 (2003).

[20] N. Keller, S. A. J. Wiegers, J. A. A. A. J. Perenboom, A. de Visser, A. A. Menovsky, and J. J. M. Franse, J. Magn. Magn. Mater. **177-181**, 298 (1998).

[21] G. J. Rozing, P. E. Mijnarends, A. A. Menovsky, and P. F. de Chatel, Phys. Rev. B **43**, 9523 (1991).

[22] J. D. S. Denlinger, G. H. Gweon, J. W. Allen, C. G. Olson, M. B. Maple, J. L. Sarrao, P. E. Armstrong, Z. Fisk, and H. Yamagami, J. Electron Spectrosc. Relat. Phenom. **117-118**, 347 (2001).

[23] G. J. Rozing, P. E. Mijnarends, and D. D. Koelling, Phys. Rev. B **43**, 9515 (1991).

[24] S. Berko, Proceedings of the International School Physics "Enrico Fermi," edited by W. Brandt and A. Dupasquier (North-Holland, Amsterdam, 1983) p. 64.

[25] E. Boroński and R. M. Nieminen, Phys. Rev. B **34**, 3820 (1986).

[26] D. G. Lock, V. H. Crisp, and R. N. West, J. Phys. F: Met. Phys. **3**, 561 (1973).

[27] J. H. Kaiser, R. N. West, and N. Shiotani, J. Phys. F: Met. Phys. **16**, 1307 (1986).

[28] A. Rubaszek, Z. Szotek, and W. M. Temmerman, Phys. Rev. B **63**, 165115 (2001).

[29] C. K. Majumdar, Phys. Rev. **140**, A227 (1965).

[30] J. Rusz, M. Biasini, and A. Czopnik, Phys. Rev. Lett. **93**, 156405 (2004).

[31] J. Rusz and M. Biasini, Phys. Rev. B **71**, 233103 (2005).

[32] P. Blaha, K. Schwarz, G. K. H. Madsen, D. Kvasnicka, and J. Luitz, WIEN2K, Vienna University of Technology, 2001.

[33] J. Rusz and M. Biasini, Phys. Rev. B **75**, 235115 (2007).

[34] M. Biasini and J. Rusz, J. Phys.: Condens. Matter **18**, L289 (2006).

[35] B. Wolf, W. Sixl, R. Graf, D. Finsterbusch, G. Bruls, B. Luthi, E. A. Knetsch, A. A. Menovsky, and J. A. Mydosh, J. Low Temp. Phys. **94**, 307 (1994).

[36] S. Elgazzar, J. Rusz, M. Amft, P. M. Oppeneer, and J. A. Mydosh, arXiv:0809.2887, Nature Mater. (to be published).

[37] M. A. Monge, M. Biasini, G. Ferro, M. Gemmi, G. Satta, S. Massidda, P. Lejay, and A. Continenza, Phys. Rev. B **65**, 035114 (2002).

[38] F. Steglich, C. Geibel, K. Gloos, G. Olesch, C. Schank, C.

Wassilew, A. Loidl, A. Krimmel, and G. R. Steward, J. Low Temp. Phys. **95**, 3 (1994).
[39] M. Biasini, M. A. Alam, H. Harima, Y. Onuki, H. M. Fretwell, and R. N. West, J. Phys.: Condens. Matter **6**, 7823 (1994).
[40] M. Biasini, G. Ferro, and A. Czopnik, Phys. Rev. B **68**, 094513 (2003).
[41] H. Yamagami and A. Hasegawa, J. Phys. Soc. Jpn. **61**, 2388 (1992); **62**, 592 (1993).
[42] We recall that for an uncompensated metal the net Fermi volume, electron part minus hole part (or vice versa), must yield 50% of the BZ volume.
[43] See, for example, S. Massidda, R. Resta, M. Posternak, and A. Baldereschi, Phys. Rev. B **52**, R16977 (1995); S. Massidda, A. Continenza, M. Posternak, and A. Baldereschi, *ibid.* **55**, 13494 (1997).
[44] H. Yamagami and N. Hamada, Physica B **284-288**, 1295 (2000).
[45] K. Kasahara, T. Iwasawa, H. Shishido, T. Shibauchi, K. Behnia, Y. Haga, T. D. Matsuda, Y. Onuki, M. Sigrist, and Y. Matsuda, Phys. Rev. Lett. **99**, 116402 (2007), and references therein.
[46] M. B. Maple, J. W. Chen, Y. Dalichaouch, T. Kohara, C. Rossel, M. S. Torikachvili, M. W. McElfresh, and J. D. Thompson, Phys. Rev. Lett. **56**, 185 (1986).
[47] E. Hassinger, G. Knebel, K. Izawa, P. Lejay, B. Salce, and J. Flouquet, Phys. Rev. B **77**, 115117 (2008).